Journal of Chemical&Engineering Data

pubs.acs.org/jced Article

Nucleic Acid Partitioning in PEG-Ficoll Protocells

Tasdiq Ahmed, Yan Zhang, Ji-Hoon Lee, Mark P. Styczynski,* and Shuichi Takayama*

Cite This: J. Chem. Eng. Data 2022, 67, 1964–1971 Read Online

ACCESS | Metrics & More | Article Recommendations | Supporting Information

ABSTRACT: The phase separation of aqueous polymer solutions is a widely used method for producing self-assembled, membraneless droplet protocells. Nonionic synthetic polymers forming an aqueous two-phase system (ATPS) have been shown to reliably form protocells that, when equipped with biological materials, are useful for applications such as analyte detection. Previous characterization of an ATPS-templated protocell did not investigate the effects of its biological components on phase stability. Here we report the phase diagram of a PEG 35k-Ficoll 400k-water ATPS at baseline and in the presence of necessary protocell components. Because the stability of an ATPS can be sensitive to small changes in composition, which in turn impacts solute partitioning, we present partitioning data of a variety of nucleic acids in response to protocell additives. The results show that the additives—particularly a mixture of salts and small organic molecules—have profound positive effects on ATPS stability and nucleic acid partitioning, both of which significantly contribute to protocell function. Our data uncovers several new areas of optimization for future protocell engineering.

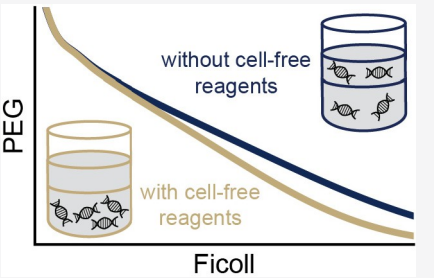

INTRODUCTION

The synthesis of artificial cells with complexity mimicking biological cells in both structure and function is an emerging frontier of synthetic biology.[1,2] The definition of a "synthetic" or "artificial" cell can vary, referring to anything from simple droplet emulsions with amorphous structure and limited functionality to a complex, compartmentalized, cell-like nonliving entity capable of reproducing cellular features. These synthetic cells are particularly promising for helping to address the question of how life began, as building a cell from organic materials is a challenge closely related to that underlying the origin of life.[3] Synthetic cells can also be used as platforms for biotechnological innovation, addressing grand challenges in medicine and diagnostics.[4,5]

Our group has previously reported the use of simple cell-like compartments, or "protocells," as multiplexable biosensors capable of executing gene expression and analyte detection tasks when interfaced with cell-free protein expression systems.[4] Protocells can be constructed in the laboratory with structures such as liposomes,[6] water-in-oil emulsions,[7] coacervates,[8] and synthetic proteinosomes.[9] Our approach uses a polymeric aqueous two-phase system (ATPS) formed from polyethylene glycol (PEG, MW 35 kDa) and Ficoll (MW 400 kDa) to create phase-separated, membraneless protocells by including the constituents and reagents needed to allow transcription, translation, and other enzymatic activities (Figure 1). Many polymers tend to be "incompatible", a characteristic that leads to aqueous polymer mixtures spontaneously demixing into distinct phases in solution.[10] This process, known as liquid–liquid phase separation, has long been hypothesized as playing a central role in the formation of early life,[11] and is now understood to be a major organizing principle within cells.[12] In our work, we use synthetic polymers such as PEG and Ficoll to form an ATPS because they are low-cost and serve as a facile method for preparing protocells. Importantly, these protocells experience minimal transport restrictions across the membraneless liquid–liquid interface.[13] This last point is particularly critical for biotechnological applications like sensors, as analytes such as nucleic acids are too large to pass through membranes.

To improve and advance our protocells and their applications, we must first better understand our current system. Our primary interest is in studying further the PEG-Ficoll ATPS that was shown to exhibit superior (compared to PEG-dextran) compartmentalization and compatibility of lysate-derived transcription and translation machinery for protein synthesis.[4] The differences observed in these two systems prompted us to investigate the PEG-Ficoll ATPS in cell-free protein expression settings in greater depth. While the PEG-Ficoll ATPS was better at preventing component mislocalization and crosstalk in a multiplexed protocell configuration, during biosensor development we found some escape of reporter molecules (green fluorescent protein, GFP) from the protocells into the surrounding environment after 3 h. This escape could have been due to breakdown of the phase separation or due to diffusion of the reporter molecules out of the protocell; each of these possibilities could complicate

Special Issue: In Honor of Joan F. Brennecke

Received: January 19, 2022
Accepted: April 25, 2022
Published: May 10, 2022

https://doi.org/10.1021/acs.jced.2c00042
J. Chem. Eng. Data 2022, 67, 1964–1971

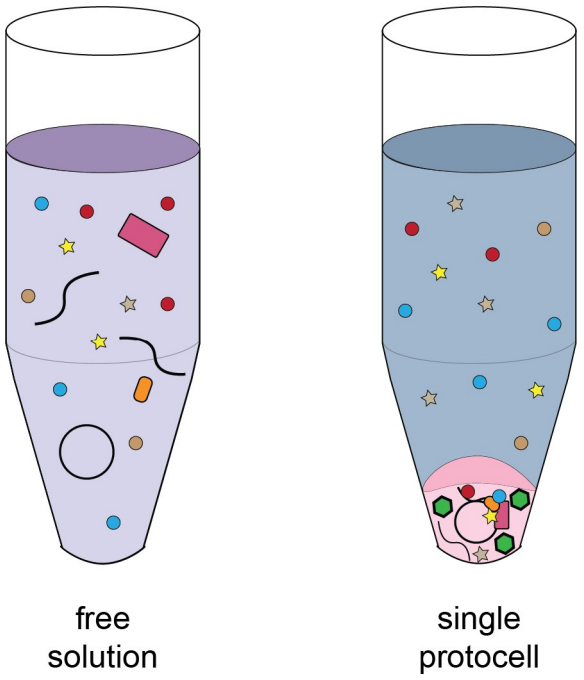

Figure 1. PEG-Ficoll protocell system under investigation, compared to a single-phase free solution. The protocell system as previously reported by our group is composed of 5%v/v PEG 35k (blue) and 10%v/v Ficoll 400k (pink). Plasmids (large circle), cell-free machinery (polymerase and ribosomes; rectangles and ovals), and Emix reaction buffer (mixture of nucleotides, amino acids and necessary cofactors; smaller circles and stars) necessary for transcription and translation reactions are included, allowing the formation of a functional protocell. When in operation, the protocell is capable of responding to an analyte (curved line) and producing a signal (GFP; green hexagons). Compartmentalization of these components into one phase of an ATPS enhances the reaction efficiency. The underlying phase system and the partitioning of nucleic acids (analyte and plasmid) are further examined and reported here.

biosensor development or deployment. The origins of these issues may be elucdiated by a proper description of the ATPS at hand, especially in the biosensor context. In this work, we examine the effect different protocell components or additives have on two-phase stability and biomolecule partitioning.

The two additives we are most interested in studying are not single molecules, but rather two collections of molecules. The first comprises the cell-free reagents needed to execute protocell functions, which is referred to as the energy mix (Emix).[14] This additive is a well-defined mixture of nucleotides, amino acids, and various salts and cofactors necessary for the transcription and translation reactions in the protocell. The second additive to consider is the biological machinery needed to execute those reactions: polymerases and ribosomes, among which protein is a primary constituent. While we directly study the impacts of the well-defined Emix composition in this work, the transcriptional and translational machinery—derived from crude cell lysate—is not used in consistently well-defined concentrations and compositions, and thus is best modeled with the economical stand-in protein bovine serum albumin (BSA). BSA is a common model protein that can mimic nonspecific effects of protein concentration; since the total protein content of the transcriptional and translational machinery in the previously published protocell system was 10 mg mL^{-1}, we used that concentration for the BSA additive in this work.

We investigate the effects these additives have on the protocell ATPS and the nucleic acids (plasmids, oligos) central to sensing functionality. Here, we show the impact of these additives on the phase separation threshold—the binodal curve on the ATPS phase diagram—of PEG and Ficoll. We also present the effect of the additives on the partitioning behavior and localization (or lack thereof) of nucleic acids that can constitute both component machinery and biosensor targets. Several unforeseen effects of the Emix likely contribute to the success of our previously reported protocells and the overall results provide insights that may help future protocell research.

EXPERIMENTAL SECTION

Materials. A pair of phase-forming polymers were used in this manuscript: polyethylene glycol (PEG) and Ficoll (both Sigma-Aldrich), with average molecular weights of 35 000 Da and 400 000 Da, respectively. Bovine serum albumin (BSA) biotechnology-grade powder and nuclease-free water were purchased from VWR Chemicals, with the latter used as the solvent for all solutions. Stock solutions of 30%w/w PEG, 40% w/w Ficoll, and 100 mg/mL BSA were prepared as needed. The energy mix (Emix) buffer, critical for protocell function, was produced in-house as needed at 3.5× stock concentration; its chemical makeup is listed in Supporting Information (SI) Table S1; all components were purchased from Sigma. For partition experiments, Emix was prepared without tRNA, as it would be detected by the general DNA stain used and thus would prevent the characterization of partitioning.

DNA. All oligos used in this study were purchased from Integrated DNA Technologies and delivered as lyophilized samples. Double-stranded oligo (Chi6) was synthesized as an Ultramer duplex to improve the full-length product yield. Working stocks were made by rehydrating oligos in nuclease-free water in accordance with the manufacturer's specifications and samples were stored at −20 °C until use. Plasmid DNA (pJL1) was prepared using EZNA maxiprep columns (OMEGA Bio-Tek) followed by isopropanol and ethanol precipitation. The purified DNA pellet was reconstituted in the elution buffer, its concentration was measured on a Nanodrop 2000 (ThermoFisher), and the sample was stored at −20 °C until use. All the DNA sequences are provided in the SI.

Cloud Point Titration Experiment. Three different conditions for polymer concentration pairings that demix into one or two phases for an ATPS were analyzed: (1) with no additives, (2) with 10 mg/mL BSA, or (3) with 1× Emix (including tRNA). Polymer stock solutions could be used as prepared for set 1, and diluted stock solutions of polymer and nuclease-free water containing the required additive concentration were prepared for sets 2 and 3. The well-established method of cloud point (turbidometric) titration was used to compile the data. Several initial points expected to fall within the two-phase region were used as starting points for a titration series. Using an analytical balance with precision of ±0.1 mg (model XS204, Mettler Toledo), precise amounts of each polymer solution were dispensed with a manual pipettor into a 15 mL Falcon centrifuge tube until the desired pair of starting concentrations were achieved. The tube was then vortexed (for several seconds) until turbidity was seen by the eye. Water was then added dropwise until the mixture formed only one phase. Then, one polymer was added dropwise to the tube until turbidity was observed again. At each stage, the mass of all

https://doi.org/10.1021/acs.jced.2c00042
J. Chem. Eng. Data 2022, 67, 1964−1971

added solutions was recorded along with the number of observed phases. Plotting all pairs with corresponding phase number resulted in a zigzag pattern that theoretically formed the bounds for the binodal curve. A few points close to the true binodal were challenging to assess, but in those situations, a centrifuge was used to enhance the settling (with >1000*g* speeds for at least 1 min), after which the phase number can be identified.

Binodal Fitting. Several fitting equations were considered for creating a binodal curve.[15] A custom Python script using the Lmfit package was written to compute model coefficients (available upon request). The Lmfit package was used because of its versatile functionalities such as efficient nonlinear optimization for complex curve fitting, simple and flexible plotting capability, and ease of handling fit statistics, all features that were instrumental in the selection process. After the initial fitting was performed, two candidates were chosen based on how well they appeared to fit the data (all of the other equations would have resulted in a nonsensical fit for at least one data set, such as traversing an axis—fits must be asymptotic at $x = 0$ and $y = 0$). The two model equations were then compared further using three statistical parameters: R-squared (R^2), root-mean-squared error (RMSE), and Akaike information criterion (AIC). These parameters were then compared to select the best fitting equation (SI Table S2).

Partition Experiments. A fluorescent DNA-binding dye, SYTOX Green (ThermoFisher), was used to measure relative amounts of DNA in the top and bottom phases of an ATPS at a fixed concentration (5%v/v PEG 35k, 10%v/v Ficoll 400k). The stain was found to emit virtually zero fluorescence when not in the presence of DNA; it was added to each mixture at a ratio of 50 bases per dye molecule.[16] In order to confirm that the top phase in our system was PEG-rich and that the bottom phase was Ficoll-rich, we prepared a stock solution of 30%w/w Ficoll 400k spiked with 0.1%w/w TRITC-Ficoll 400k (Sigma-Aldrich). We then produced initial ATPS mixtures using this fluorescent Ficoll stock to confirm the orientation of the phases; all partition experiments used nonfluorescent Ficoll, as the TRITC fluorescence spectrum overlaps with SYTOX Green. There were five test conditions for each DNA of interest: (1) a control group with the DNA in nuclease-free water, (2) an ATPS reference group with DNA, (3) an ATPS group with Emix in solution, (4) an ATPS group with BSA added, and (5) an ATPS group with both additives present. The control ATPS-free group was necessary to confirm that any partitioning of DNA to the bottom phase was because of affinity and not gravity. For each condition, all components were dispensed into a tube sequentially (in no designated order) before thoroughly mixing by manual pipettor, until complete and homogeneous turbidity was observed. Six tubes were used for each condition, except in the case of the high GC-content hairpin oligo, which only used three replicates. Because the settling time for the chosen ATPS is at least several hours, mixtures were prepared at room temperature before placing in a 4°C refrigerator overnight to minimize DNA degradation. The next day, samples were warmed at room temperature before careful extraction of 60 μL of each phase by pipettor into a black-walled, clear-bottomed 96-well plate (Corning). Tubes were tilted such that the liquid−liquid interface would be exposed to air, allowing for minimal interaction with the top phase when attempting to draw liquid from the bottom phase. Fluorescence intensities were not found to be different using this method when compared to using syringe needles to puncture the tube for bottom phase recovery (data not shown). All fluorescence measurements were collected using a Synergy H4 microplate reader (BioTek Instruments), which has an accuracy of ±1%. The uncorrected partition coefficients K were calculated as $K = \frac{I_{top}}{I_{bottom}}$, where I represents the fluorescence intensity of a single phase. The measurement uncertainty for each reported partition coefficient is ±2%.

Statistical Analysis. A one-way Brown-Forsythe and Welch's ANOVA, in which the homogeneity of variances is not required to be valid, was performed in GraphPad Prism to compare the effect of additives on partition coefficients. Upon finding any statistically significant differences between at least two groups, a Tukey's post hoc test at a confidence interval of 95% was used to find specific differences in partition coefficients between the groups. A Bonferroni correction was applied to the p-values to account for multiple comparisons accordingly. The results were then plotted as individual points with mean ± SD.

RESULTS AND DISCUSSION

We focused on measuring two important aspects of our protocells used for biosensing applications: the polymer ATPS comprising the sensor, and the nucleic acids serving as analytes (short oligonucleotides) and components of the sensing process (plasmids).

ATPS Binodal Determination. Our initially reported protocells are set at nonequilibrium concentrations of 5%v/v PEG 35k and 10%v/v Ficoll 400k in nuclease-free water. These concentrations sit well above the binodal curve and will reliably phase separate, which is why they were chosen as the standard pairing for our protocells. Deeper understanding of the ATPS's stability when interfaced with protocell constituents, which will in turn enable improved engineering of the system, requires a broader mapping of the underlying liquid−liquid equilibria. The PEG-Ficoll ATPS is an understudied system, with few phase diagrams reported previously.[10,17,18] Interestingly, in these reports the binodal curve has an irregular shape deviating from the typical bell-like shape commonly observed for an ATPS, with the "elbow" of the curve shifted closer to the PEG axis. Furthermore, previously measured PEG-Ficoll ATPS tie lines did not connect points on the binodal curve found with traditional cloud point titration,[17] a phenomenon hypothesized to result from potential polydispersity within the Ficoll solution,[10] although such effects are not seen in a dextran-Ficoll phase diagram.

We performed cloud point titration experiments to map the phase separation behavior at room temperature of a PEG 35k-Ficoll 400k system, with nuclease-free water as the solvent. The temperature of the protocells when used for sensing functionality can range from room temperature to 37°C. Since temperature changes typically induce binodal curve shifts, we characterized the binodal only at room temperature to obtain a first-pass diagram. Three sets of data were needed, as we sought to determine if the two key additives, Emix and BSA, have individual effects on binodal curve position.

Phase diagram data are provided in Tables 1, 2, and 3, with fitted binodal curves plotted along with the data points in Figure 2. From an initial pool,[15] we considered two nonlinear fitting equations for comparison, the first from Merchuk and colleagues[19] which is the most commonly used model for plotting ATPS binodals, and the second from Hu and co-

https://doi.org/10.1021/acs.jced.2c00042
J. Chem. Eng. Data 2022, 67, 1964−1971

Table 1. Binodal Data for PEG-Ficoll-Water ATPS with No Additional Additives[a]t

one-phase		two-phase	
PEG %(w/w)	Ficoll %(w/w)	PEG %(w/w)	Ficoll %(w/w)
0.69	19.07	1.14	18.48
1.06	17.13	1.53	16.38
1.19	16.55	1.57	16.08
1.37	16.01	1.77	14.83
1.43	14.72	2.10	13.16
1.94	12.98	2.29	12.56
1.97	13.29	2.62	10.96
2.20	12.09	2.79	10.37
2.21	11.91	2.96	9.81
2.71	9.09	2.99	9.68
2.98	8.01	3.10	9.21
3.10	7.60	3.12	8.76
3.35	6.77	3.23	8.86
3.48	6.23	3.30	8.09
3.76	5.02	3.30	8.60
3.90	4.45	3.40	7.74
4.19	3.74	3.51	7.34
4.50	2.43	3.67	6.58
4.74	1.79	3.81	6.22
5.02	1.28	3.86	5.75
5.14	0.99	4.01	5.20
5.36	0.74	4.21	4.82
		4.34	3.88
		4.71	2.54
		6.17	0.36
		6.71	0.30

[a]Solvent is nuclease-free water; experiment was performed at room temperature. Standard uncertainty u = 0.001 for each phase measuremen.

Table 2. Binodal Data for PEG-Ficoll-Water ATPS with 10 mg mL^{-1} BSA[a]

one-phase		two-phase	
PEG %(w/w)	Ficoll %(w/w)	PEG %(w/w)	Ficoll %(w/w)
0.48	5.54	0.98	18.01
0.52	5.36	1.22	16.68
0.73	5.19	1.38	15.95
0.94	5.14	1.53	15.29
1.29	4.88	1.61	14.83
2.14	4.64	1.69	14.60
2.77	4.47	1.73	14.46
3.55	4.26	1.86	14.04
4.01	4.15	1.97	13.41
4.98	3.84	2.11	12.93
7.89	3.16	2.23	12.52
8.39	3.03	2.31	12.12
9.01	2.88	2.88	9.42
9.76	2.63	3.08	8.69
9.93	2.59	3.23	8.07
11.51	2.26	3.37	7.74
11.74	2.24	3.50	7.31
12.31	2.08	3.89	5.45
12.58	2.05	4.05	4.64
13.19	1.89	4.51	3.07
13.71	1.83	5.77	0.56
14.21	1.70	6.21	0.40
14.62	1.59	6.42	0.34
16.47	1.20	6.70	0.35
17.01	1.10		
17.55	0.96		
18.69	0.65		

[a]Solvent is nuclease-free water; experiment was performed at room temperature. Standard uncertainty u = 0.001 for each concentration measurement.

workers.[20] Statistical analyses were performed on these models with our phase data as input, and the results are presented in SI Table S2. We found that the second equation provides a better fit qualitatively and with respect to the three tabulated statistical criteria. Specifically, the second model has an R^2 closer to 1.0, a lower RMSE, and a more negative AIC, all values that support the notion that the more expansive second nonlinear model is the best choice. The most striking observation from the plotted curves is that while BSA appears to have very little influence on the binodal in shifting from its base additive-free position, Emix has a substantial effect. Rather than produce a unidirectional shift across the entire concentration range, Emix appears to have greater influence on the binodal as the Ficoll concentration increases. Additionally, the fit suggests that the Emix curve may have a crossover point where at the Ficoll concentration below this point, there is a decreased tendency to phase separate relative to an additive-free mixture. However, the range of concentrations where one would find phase separation without Emix but not with Emix is narrow, and after testing several points near this range, we cannot confirm the existence of a crossover point (SI Table S3). Nonetheless, the phenomenon of Ficoll-dependent drift, which is confirmed in SI Figure S1, demonstrates that Emix alters the solution properties such that phase separation is affected. We note that in practice, the volume ratio of the mixtures changes upon Emix introduction, such that the Ficoll-rich phase grows.

Nucleic Acid Partitioning. The other arm of investigation focused on the nucleic acids central to the protocell system and how they may interact with the different system components. Plasmids are components in the sensing process, serving as the template for expression of molecular sensing domains and for target-modulated expression of reporters that indicate analyte detection. Small oligonucleotides serve as models for analytes that may be present in single- or double-stranded forms. We assessed partitioning at a fixed set of concentrations (5%v/v PEG 35k, 10%v/v Ficoll 400k), selected to be consistent with our previously reported protocells and thus potentially relevant for future applications. Partitioning bias can decrease as a system moves closer to a binodal,[10] so it was important to make sure our polymers are concentrated enough that we would be able to observe nucleic acid partitioning. As mentioned above, all experiments were performed with nuclease-free water as a solvent to minimize degradation of the nucleic acids. Partition coefficients were calculated as a ratio of top phase to bottom phase fluorescence, using absolute fluorescence intensities of the DNA intercalating dye SYTOX Green, which only emits light when bound to DNA. Traditional spectrophotometric measurements of DNA concentration cannot be used for nucleic acid quantification because ATPS polymers interfere with absorbance readings at 260 nm. We also note that the partition experiments used Emix prepared without tRNA, as it binds to the dye.

https://doi.org/10.1021/acs.jced.2c00042
J. Chem. Eng. Data 2022, 67, 1964−1971

Table 3. Binodal Data for PEG-Ficoll-Water ATPS with 1× Concentrate Emix[a]

one-phase		two-phase	
PEG %(w/w)	Ficoll %(w/w)	PEG %(w/w)	Ficoll %(w/w)
0.38	18.74	0.57	18.12
0.59	17.10	0.68	16.99
0.68	16.42	0.74	16.35
0.75	15.70	1.19	14.08
0.90	14.88	1.27	13.70
0.92	15.24	1.30	13.98
0.97	14.59	1.44	13.31
0.98	14.90	1.53	12.90
1.15	13.58	1.84	12.14
1.31	13.43	1.95	11.65
1.49	12.54	1.98	11.45
1.78	11.75	2.05	11.17
1.90	11.30	2.17	10.95
2.05	10.24	2.40	9.96
2.07	10.48	2.46	9.53
2.32	8.97	2.87	8.37
2.79	8.14	3.20	7.63
2.91	7.82	3.38	7.00
3.20	6.62	3.53	6.44
3.33	6.35	3.71	5.63
3.50	5.65	4.13	5.03
3.93	4.78	4.17	3.89
4.16	2.81	4.37	4.08
4.30	3.48	4.45	3.60
4.53	2.32	4.56	3.08
4.83	1.89	4.94	1.93
4.90	1.42	5.05	1.98
5.20	1.00	5.11	1.48
5.24	1.10	5.41	1.13
5.39	0.88	5.55	1.06
5.51	0.70	5.87	0.75
		6.16	0.61

[a]Solvent is nuclease-free water; experiment was performed at room temperature. Standard uncertainty u = 0.001 for each concentration measurement.

We first examined the partitioning behavior of ssDNA oligos. Two oligos were synthesized: (1) a flexible 40 nt oligo consisting of 10× ACTG repeats and no expected secondary structure, and (2) a structured 40 nt oligo with sequence designed to form a hairpin loop, and with equivalent (50%) GC content to the first oligo. Both oligos were independently tested for their ability to partition in our ATPS of interest. Uncorrected partition coefficients K (and statistics) for each oligo in each condition are listed in SI Tables S4 and S5. For the flexible oligo, there is mostly negligible partitioning when placed in an ATPS (Figure 3). It is only in the presence of Emix that K-values show a significant decrease, where the oligo favors the bottom Ficoll-rich phase. This is in agreement with our initial expectation of no phase bias for a DNA molecule of this size. However, incorporation of a structural element into the oligo does appear to strongly influence partitioning (Figure 4). BSA contributes to a decrease in K in comparison to the control, but the addition of Emix further enhances partitioning with the ATPS+Emix condition at K = 0.3801 (n = 6, p < 0.0001). We also explored whether nucleotide sequence content would modulate partitioning, as we had hairpin oligos with 67.5% GC-content (SI Figure S2). Both hairpin oligos demonstrate appreciable increases in Ficoll-phase localization, but the most noticeable change is in the effect of BSA, which is more pronounced in the higher GC-content oligonucleotide. A physicochemical rationale for lower K-values in the BSA group is not immediately obvious, since the dual-additive condition has (insignificantly) weaker partitioning compared to the Emix condition. This large BSA-induced shift does suggest that there exists a relationship between GC-richness and the impact of BSA. The dual-additive conditions also raise the possibility that Emix may interact with and tune the partitioning behavior of BSA itself, and vice versa, when one considers that the dual condition almost always results in K-values slightly higher than for the Emix-only condition.

We next assessed the partitioning of duplex DNA to further evaluate the role structure may have on partitioning. A Chi6 dsDNA molecule with 86 nt long sense and antisense strands was tested (Figure 5). In line with the ssDNA oligo data, Chi6 also has marked decreases in K, with nearly 95% of the duplex favoring the bottom phase in both mixtures containing Emix. Interestingly, BSA does enhance partitioning to similar levels as the higher GC-content oligo.

The size effect is clear after examining the partitioning for a plasmid (pJL1, ∼2.4 kb in length) in our protocell ATPS (Figure 6). For 10 nM of plasmid, partitioning into the Ficoll-rich phase exceeds 99%, with a 4-fold decrease in K for the ATPS+BSA group relative to Chi6. Yet, the most puzzling observation from both Chi6 and pJL1 experiments is the unexpected reversal in partitioning for the ATPS-only condition. At worst, one would expect dsDNA to spread evenly between two phases without any additional components introduced, with likely a greater—if only slightly—preference for the hydrophilic Ficoll phase. The ATPS-only result seen in Figure 6 has been reproduced multiple times with K > 1. One may have to consider the effect intercalating dyes have on DNA, namely that dyes such as SYTOX can induce lengthening[21,22] and supercoiling,[23] which in turn may affect the phase preference. It was previously shown in a PEG-dextran ATPS that nucleic acids will respond similarly significantly by changing the phase preference in the presence of various common salts.[24] While our focus is solely on effects induced by the small molecules present in our protocell, we anticipate that similar effects from these external salts will occur. The partitioning work described here collectively leads us to conclude that the effects of small molecule additives are not negligible, and that both the additive composition and DNA sequence and structure are important for protocell function and are parameters to be explored for future improvements in function.

CONCLUSIONS

For nonionic polymers forming an ATPS, salts do not typically have a significant effect on phase separation until they approach molar amounts.[10,25] Because the concentrations of the individual components of the Emix buffer are mostly in millimolar ranges, the observed binodal curve shifts were not expected. Rather, we anticipated BSA to have some effect, as BSA is itself a phase-forming polymer,[26] and we have previously shown that adding low concentrations of a third polymer to an ATPS can considerably lower the threshold to phase separation, even if the third polymer does not segregate into its own distinct phase.[18] The effect of Emix has a few implications we envision as being impactful beyond the specific protocell configuration studied here. First, because the Emix

https://doi.org/10.1021/acs.jced.2c00042
J. Chem. Eng. Data 2022, 67, 1964−1971

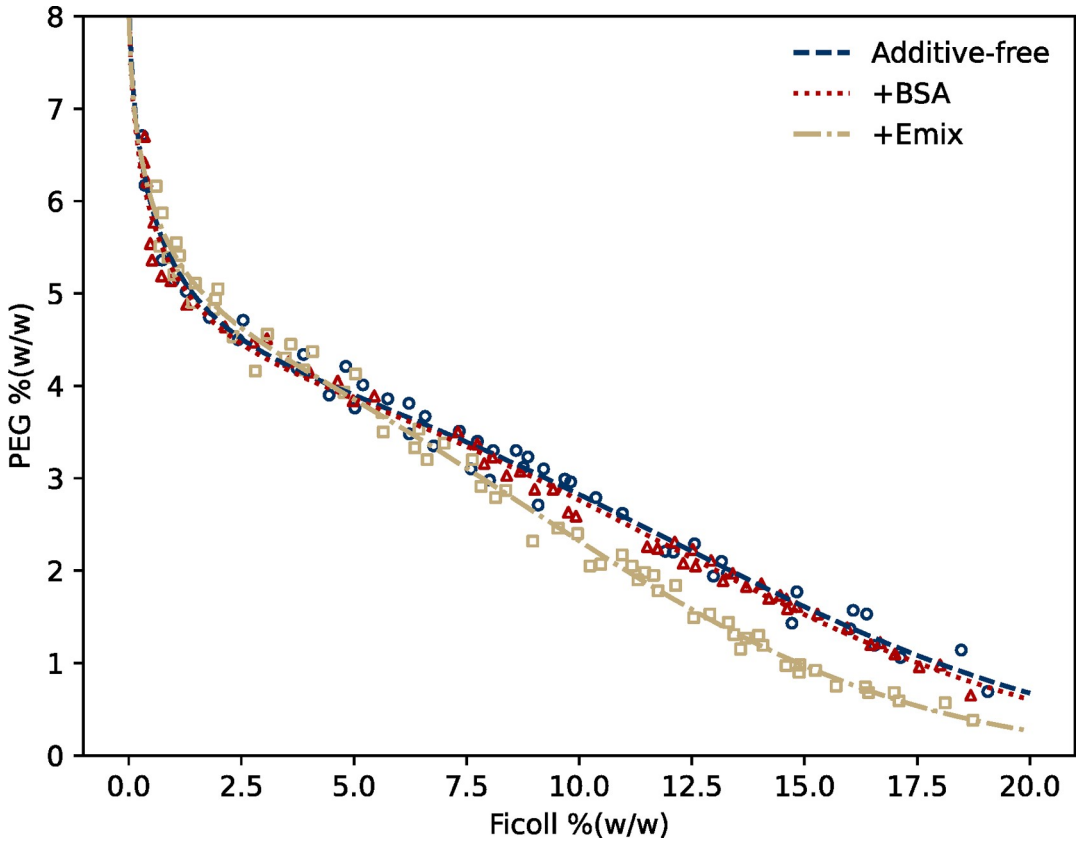

Figure 2. Binodal curves for a PEG 35k–Ficoll 400k ATPS: (blue line/circles) with no additive, (red line/triangles) with 10 mg mL^{-1} BSA, (gold line/squares) with 1× concentrate Emix. Individual points that approximate the binodal are presented in corresponding colors.

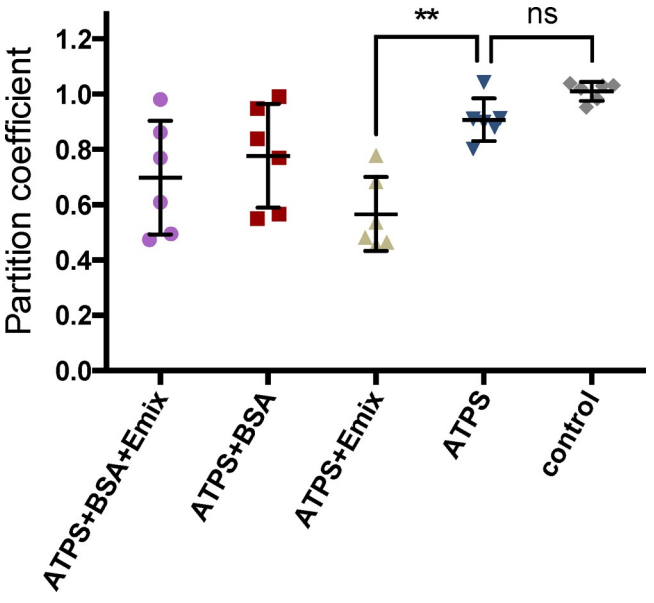

Figure 3. Partition data of flexible 10× ACTG ssDNA, at 1 μM. (left–right) with BSA and Emix, with BSA, with Emix, no additive, ATPS-free control; n = 6. Significant changes in K only occur when Emix is present. Data shown as individual points with mean ± SD.

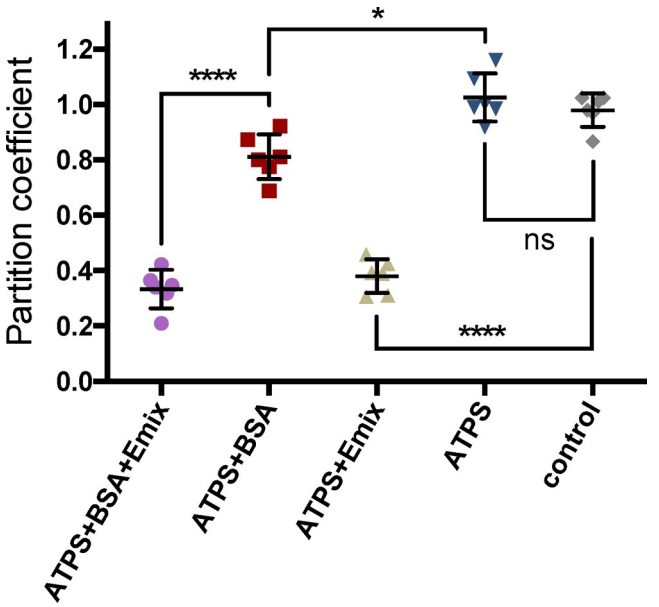

Figure 4. Partition data of hairpin ssDNA with 50% GC-content, at 1 μM. (l-r) with BSA and Emix, with BSA, with Emix, no additive, ATPS-free control; n = 6. The addition of a structural element strongly improves DNA localizing to the Ficoll-rich phase, with the effect of Emix significantly enhanced. Data shown as individual points with mean ± SD.

composition can be varied while still allowing gene expression functionality, specific formulations may be engineered for different applications (such as biochemical extraction, nucleic acid delivery, or cell patterning), thus providing new opportunities for optimization. In addition, considering that the Emix was designed to mimic the intracellular environment so that the transcription–translation reactions can operate effectively, it is possible that differences in the small molecule

https://doi.org/10.1021/acs.jced.2c00042
J. Chem. Eng. Data 2022, 67, 1964–1971

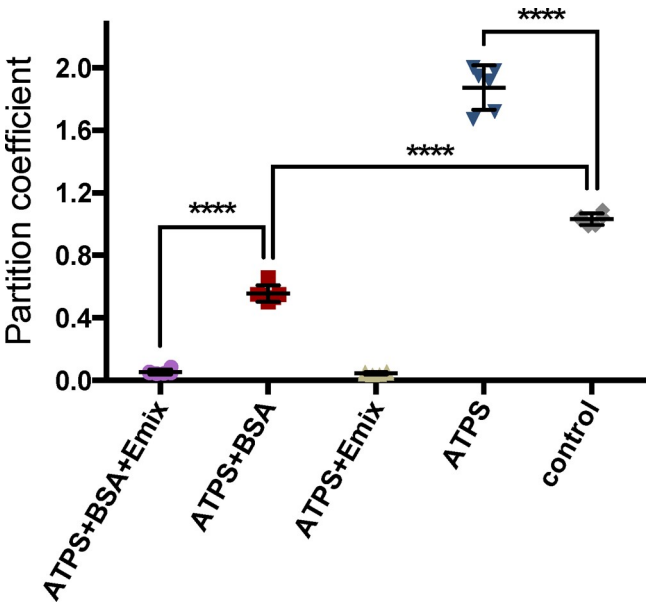

Figure 5. Partition data of Chi6 dsDNA, at 2 μM. (l-r) with BSA and Emix, with BSA, with Emix, no additive, ATPS-free control; n = 6. Chi6 almost entirely partitions into the Ficoll-rich phase when Emix is present. Data shown as individual points with mean ± SD.

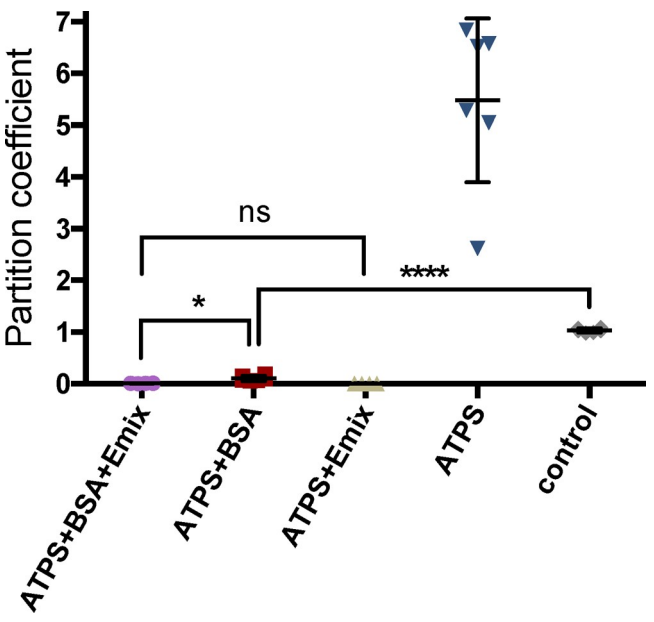

Figure 6. Partition data of pJL1 plasmid, at 10 nM. (l-r) with BSA and Emix, with BSA, with Emix, no additive, ATPS-free control; n = 6. Additives continue to correlate with low K, approaching almost total partitioning. However, dsDNA appears to prefer PEG when no additives are present. Data shown as individual points with mean ± SD.

makeup of intracellular environments may play a role in regulating liquid−liquid phase separation in cells. Moreover, the local milieu may enhance the partitioning of critical or substrate macromolecules into functionalized liquid compartments. Further work is needed to address these hypotheses, but a few applications incorporating the findings presented here can likely be achieved in the short term.

■ ASSOCIATED CONTENT

Supporting Information

The Supporting Information is available free of charge at https://pubs.acs.org/doi/10.1021/acs.jced.2c00042.

Figure S1, confirmation of an Emix-induced binodal shift; Figure S2, partition data of hairpin ssDNA with 67.5% GC-content; Table S1, Emix composition; Table S2, coefficients; statistical comparison of two model fitting equations; Table S3, crossover region examination; Table S4, DNA partition coefficients; Table S5, partition coefficient p-values and significance; and DNA sequence information (PDF)

■ AUTHOR INFORMATION

Corresponding Authors

Mark P. Styczynski − *School of Chemical & Biomolecular Engineering, Georgia Institute of Technology, Atlanta, Georgia 30332, United States;* orcid.org/0000-0002-1479-6658; Email: Mark.Styczynski@chbe.gatech.edu

Shuichi Takayama − *Wallace H. Coulter Department of Biomedical Engineering and Petit Institute for Bioengineering and Bioscience, Georgia Institute of Technology and Emory School of Medicine, Atlanta, Georgia 30332, United States;* orcid.org/0000-0002-4385-9080; Email: takayama@gatech.edu

Authors

Tasdiq Ahmed − *Wallace H. Coulter Department of Biomedical Engineering and Petit Institute for Bioengineering and Bioscience, Georgia Institute of Technology and Emory School of Medicine, Atlanta, Georgia 30332, United States*

Yan Zhang − *School of Chemical & Biomolecular Engineering, Georgia Institute of Technology, Atlanta, Georgia 30332, United States;* orcid.org/0000-0003-0719-5456

Ji-Hoon Lee − *Wallace H. Coulter Department of Biomedical Engineering and Petit Institute for Bioengineering and Bioscience, Georgia Institute of Technology and Emory School of Medicine, Atlanta, Georgia 30332, United States;* orcid.org/0000-0002-3542-3885

Complete contact information is available at: https://pubs.acs.org/10.1021/acs.jced.2c00042

Notes

The authors declare no competing financial interest.

■ ACKNOWLEDGMENTS

We thank Dr. Michael Jewett for his gift of the pJL1 plasmid used in this study. M.P.S. and S.T. thank the National Institutes of Health (MPS: R01EB022592; ST: R01HL136141, R01GM123517 & R21AG061687) for their support.

■ REFERENCES

(1) Xu, C.; Hu, S.; Chen, X. Artificial cells: from basic science to applications. *Mater. Today* **2016**, *19* (9), 516−532.

(2) Dzieciol, A. J.; Mann, S. Designs for life: protocell models in the laboratory. *Chem. Soc. Rev.* **2012**, *41* (1), 79−85.

(3) Poudyal, R. R.; Pir Cakmak, F.; Keating, C. D.; Bevilacqua, P. C. Physical Principles and Extant Biology Reveal Roles for RNA-Containing Membraneless Compartments in Origins of Life Chemistry. *Biochemistry* **2018**, *57* (17), 2509−2519.

(4) Zhang, Y.; Kojima, T.; Kim, G.-A.; McNerney, M. P.; Takayama, S.; Styczynski, M. P. Protocell arrays for simultaneous detection of diverse analytes. *Nat. Commun.* **2021**, *12* (1), No. 5724.

(5) Sato, W.; Zajkowski, T.; Moser, F.; Adamala, K. P. Synthetic cells in biomedical applications. *WIREs Nanomed. Nanobiotechnol.* **2022**, *14* (2), No. e1761.
(6) Nourian, Z.; Danelon, C. Linking Genotype and Phenotype in Protein Synthesizing Liposomes with External Supply of Resources. *ACS Synth. Biol.* **2013**, *2* (4), 186−193.
(7) Torre, P.; Keating, C. D.; Mansy, S. S. Multiphase water-in-oil emulsion droplets for cell-free transcription−translation. *Langmuir* **2014**, *30* (20), 5695−5699.
(8) Koga, S.; Williams, D. S.; Perriman, A. W.; Mann, S. Peptide−nucleotide microdroplets as a step towards a membrane-free protocell model. *Nat. Chem.* **2011**, *3* (9), 720−724.
(9) Huang, X.; Li, M.; Green, D. C.; Williams, D. S.; Patil, A. J.; Mann, S. Interfacial assembly of protein−polymer nano-conjugates into stimulus-responsive biomimetic protocells. *Nat. Commun.* **2013**, *4* (1), No. 2239.
(10) Albertsson, P.-Å. *Partition of Cell Particles and Macromolecules*. 3rd ed.; Wiley: New York, 1986; p 346.
(11) Oparin, A. I. *The Origin of Life*. 2nd ed.; Dover Publications: New York, 1953; p 270.
(12) Banani, S. F.; Lee, H. O.; Hyman, A. A.; Rosen, M. K. Biomolecular condensates: organizers of cellular biochemistry. *Nat. Rev. Mol. Cell Biol.* **2017**, *18* (5), 285−298.
(13) Münchow, G. t.; Schönfeld, F.; Hardt, S.; Graf, K. Protein diffusion across the interface in aqueous two-phase systems. *Langmuir* **2008**, *24* (16), 8547−8553.
(14) Kwon, Y.-C.; Jewett, M. C. High-throughput preparation methods of crude extract for robust cell-free protein synthesis. *Sci. Rep.* **2015**, *5* (1), No. 8663.
(15) Alvarez-Guerra, E.; Ventura, S. P. M.; Alvarez-Guerra, M.; Coutinho, J. A. P.; Irabien, A. Modeling of the binodal curve of ionic liquid/salt aqueous systems. *Fluid Phase Equilib.* **2016**, *426*, 10−16.
(16) Roth, B. L.; Poot, M.; Yue, S. T.; Millard, P. J. Bacterial viability and antibiotic susceptibility testing with SYTOX green nucleic acid stain. *Appl. Environ. Microbiol.* **1997**, *63* (6), 2421−2431.
(17) Croll, T.; Munro, P. D.; Winzor, D. J.; Trau, M.; Nielsen, L. K. Analysis of the Phase Behavior of the Aqueous Poly(ethylene glycol)-Ficoll System. *Biotechnol. Prog.* **2003**, *19* (4), 1269−1273.
(18) Kojima, T.; Lin, C. C.; Takayama, S.; Fan, S. K. Determination of aqueous two-phase system binodals and tie-lines by electrowetting-on-dielectric droplet manipulation. *ChemBioChem.* **2018**, *20* (2), 270−275.
(19) Merchuk, J. C.; Andrews, B. A.; Asenjo, J. A. Aqueous two-phase systems for protein separation. *Journal of Chromatography B: Biomedical Sciences and Applications* **1998**, *711* (1−2), 285−293.
(20) Hu, M.; Zhai, Q.; Liu, Z.; Xia, S. Liquid−Liquid and Solid−Liquid Equilibrium of the Ternary System Ethanol + Cesium Sulfate + Water at (10, 30, and 50) °C. *Journal of Chemical & Engineering Data* **2003**, *48* (6), 1561−1564.
(21) Sischka, A.; Toensing, K.; Eckel, R.; Wilking, S. D.; Sewald, N.; Ros, R.; Anselmetti, D. Molecular Mechanisms and Kinetics between DNA and DNA Binding Ligands. *Biophys. J.* **2005**, *88* (1), 404−411.
(22) Thakur, S.; Cattoni, D. I.; Nöllmann, M. The fluorescence properties and binding mechanism of SYTOX green, a bright, low photo-damage DNA intercalating agent. *Eur. Biophys. J.* **2015**, *44* (5), 337−348.
(23) Ganji, M.; Kim, S. H.; van der Torre, J.; Abbondanzieri, E.; Dekker, C. Intercalation-Based Single-Molecule Fluorescence Assay To Study DNA Supercoil Dynamics. *Nano Lett.* **2016**, *16* (7), 4699−4707.
(24) Albertsson, P.-Å. Partition studies on nucleic acids: I. Influence of electrolytes, polymer concentration and nucleic acid conformation on the partition in the dextran-polyethylene glycol system. *Biochim. Biophys. Acta* **1965**, *103* (1), 1−12.
(25) Zaslavsky, B. Y.; Miheeva, L. M.; Aleschko-Ozhevskii, Y. P.; Mahmudov, A. U.; Bagirov, T. O.; Garaev, E. S. Distribution of inorganic salts between the coexisting phases of aqueous polymer two-phase systems. *Journal of Chromatography A* **1988**, *439* (2), 267−281.
(26) Edmond, E.; Ogston, A. G. An approach to the study of phase separation in ternary aqueous systems. *Biochem. J.* **1968**, *109* (4), 569−576.

https://doi.org/10.1021/acs.jced.2c00042
J. Chem. Eng. Data 2022, 67, 1964−1971